Scientific Journal for Damietta Faculty of Science **15**(2) 2025, 182-191
Doi: 10.21608/sjdfs.2025.399892.1240
ISSN Print 2314-8594
ISSN Online 2314-8616

https://sjdfs.journals.ekb.eg/

Chaotic Motion of an Electrodynamic Tethered Satellite System under Oblateness Effect in a Circular Orbit

A. Yousof*[1], A.M. Abdelaziz[2], Abd El Hakeem Abd El Naby[1] and Yehia A. Abdel-Aziz[2]

[1]Damietta University, Mathematics Department, Damietta, Egypt.
[2]National Research Institute of Astronomy and Geophysics (NRIAG), Cairo, Egypt.

Received: 01 July 2025 /Accepted: 10 July 2025

*Corresponding author's E-mail: A.usf@du.edu.eg

Abstract

This paper investigates the chaotic behavior of an in-plane electrodynamic tethered satellite system (EDTSS) operating in a circular orbit under the influence of Earth's oblateness, represented by the J_2 zonal harmonic. The system is modelled using the dumbbell model, consisting of two point masses connected by an inelastic tether. The equations of motion are derived through the Lagrangian formulation, incorporating the effects of the Lorentz force generated by the current interacting with Earth's magnetic field and the radial acceleration due to the oblateness of Earth. To analyze the conditions under which chaos may arise, the Melnikov method is applied, leading to the identification of a necessary condition for the occurrence of chaotic motion. Based on this condition, the parameter domains that are likely to result in chaotic behavior are determined. To confirm the analytical findings, numerical simulations are conducted and discussed. The results highlight the critical role of the oblateness effect and its interaction with electrodynamic forces in governing the nonlinear dynamics of tethered satellite systems.

Keywords: Chaos; Electromagnetic Force; Melnikov Analysis; Poincaré Section; Tethered Satellite System.

Introduction

Space tether systems are a promising solution for enabling highly efficient and low-cost space operations, including debris removal (Ma X and Wen H, (2023) ; Razzaghi P et al., (2021) ; Svotina V and Cherkasova M, (2023)), energy generation (Liu J et al., (2020) ; Liu J and Mcinnes CR, (2019) ; Hu W et al., (2018)), and asteroid exploration (Mashayekhi MJ and Misra AK, (2016) ; Zhong R and Wang Y, (2018)). As space activities expand, these systems offer a sustainable and effective approach to future mission design. Thus, the tethered satellite system (TSS) has emerged as one of the most active areas of research in space sciences (Huang P et al., (2018) ; Sanmartin JR et al., (2010) ; Kumar K, (2006) ; Modi V et al., (1990) ; Sánchez-Arriaga G et al., (2024)). A typical TSS consists of two or more satellites

connected by a tether element. Extensive studies have focused on these systems' modelling, dynamics, and control (Hong AaT et al., (2024) ; Andrievsky B et al., (2022)). Both Newtonian and Lagrangian mechanics are commonly applied to derive the equations of motion, with either orbital elements or libration angles used to represent the system states. The tether itself is modelled in various ways, either as massless or massive, rigid or flexible, depending on the objectives and assumptions specific to each study (Aslanov V and Ledkov A, (2012) ; Troger H et al., (2010)).

The dynamics of a tethered satellite mission are significantly influenced by various environmental perturbations that must be carefully considered during modeling and control design. Among the most prominent perturbing forces are aerodynamic drag, which is particularly relevant in low Earth orbits; solar radiation pressure, which induces subtle but continuous force variations; and the oblateness of the Earth, represented by the J_2 zonal harmonic, which alters the gravitational field and affects orbital stability. In addition to these, other perturbations such as third-body gravitational influences and magnetic torques may also impact the system depending on the mission profile. Accounting for these forces is essential to accurately predict system behaviour and ensure the success and longevity of tethered satellite operations.

Given the critical role of Earth's oblateness, represented by the J_2 coefficient, many researchers have explored its influence on orbital and tethered system behaviour. Zheng P et al., (2008) developed a mathematical model using Lagrangian mechanics and numerical simulations to analyse the deployment of a tether-assisted deorbit system under Earth's J_2 perturbation. Their results showed that J_2 mainly affects in-plane motion during deployment, without inducing out-of-plane motion when the initial out-of-plane angle is zero. Yu B and Jin D, (2010) modelled a viscoelastic tethered satellite system and examined the effects of J_2 and thermal perturbations. They found that J_2 significantly affects deployment, especially with friction, while thermal effects mainly influence retrieval, resulting in distinct motion behaviours. Yu B et al., (2016) extended the analysis of a flexible tethered satellite system under additional perturbations, including air drag, solar radiation pressure, and orbital eccentricity. Using a simplified two-degree-of-freedom model, they conducted numerical simulations that revealed bifurcations, quasi-periodic oscillations, and chaotic motions. They concluded that J_2 perturbation and thermal effects strongly influence pitch dynamics and must be considered, while air drag and solar pressure have a lesser impact depending on orbital altitude. Yu B et al., (2020) applied Melnikov analysis to determine the conditions under which chaotic motion arises in a tethered satellite system operating in a circular orbit. Their study considered the combined effects of Earth's J_2 perturbation and aerodynamic drag, showing that these perturbations can induce chaotic dynamics even when the tether is modelled as rigid. Yuan W et al., (2024) studied the chaotic motion of a tether-sail system in polar orbits, considering J_2 perturbation and orbital eccentricity. Using Lagrangian modelling and Melnikov analysis, they showed that both J_2 and eccentricity enhance chaotic behaviour.

Electrodynamic tethers (EDTs) provide key advantages over traditional tether systems by generating Lorentz forces without propellant, enabling efficient orbit control and power generation. Studies have examined the impact of Earth's J_2 perturbation on EDT dynamics. Tikhonov A et al., (2017) showed that an electrodynamic control system can effectively counteract gravity gradient torque caused by J_2 in near-Earth orbits.

To the best of our knowledge, no previous study has analytically examined the impact of Earth's oblateness (J_2 perturbation) on the dynamics of electrodynamic tethered satellite systems. Therefore, this paper aims to fill this gap by focusing on the analytical characterization of such effects. The paper is organized as follows: In Section 2, the system is modelled as a dumbbell model with non-negligible tether mass, and the equations of motion are derived using the Lagrangian approach. In Section 3, the analytical Melnikov method is applied to identify conditions under which chaotic motion may occur. Section 4 presents numerical simulations that validate the analytical results. Finally, the conclusions are discussed in Section 5.

Mathematical Model

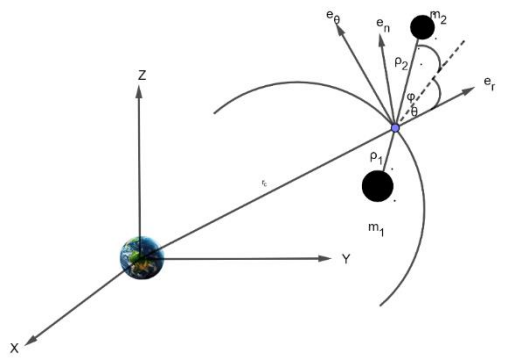

Fig. 1 Tethered Satellite System

Consider a tethered satellite system (TSS) orbiting Earth in a circular orbit, as shown in Fig. 1. A dumbbell model describes a TSS, which consists of a mother satellite connected to a subsatellite with a tether, where m_1, m_2, and m_t are their masses, respectively.

An inertial frame, (X, Y, Z), is considered, which is centered at Earth's center. The X -axis is oriented toward the vernal equinox, the Z -axis aligns with Earth's rotation axis, and the Y -axis lies within Earth's equatorial plane, maintaining a right-handed coordinate system.

A rotating frame, (e_r, e_θ, e_n), centered at system's mass center, has a relative position vector to the inertial frame, $\boldsymbol{r}_c$. The three unit vectors, (e_r, e_θ, e_n), points radially outward opposite to Earth's center of mass, oriented along the velocity direction, and completes the right-handed coordinate triad, respectively.

The mother satellite and subsatellite have position vectors relative to the system's mass center, $\boldsymbol{\rho_1}$ and $\boldsymbol{\rho_2}$, respectively. The variable θ represents the in-plane angle, while l denotes the tether length at any given time.

Suitable expressions for both kinetic and potential energies are essential for developing the system's Lagrangian. By integrating kinetic energy over the tether length and adding the kinetic energies of both the mother satellite and the subsatellite, one can obtain the total kinetic energy, T, as follows Aslanov V and Ledkov A, (2012)

$$T = \frac{1}{2} m \dot{\boldsymbol{r}}_c . \dot{\boldsymbol{r}}_c + \frac{1}{2} \mu_e (\dot{l}^2 + l^2 (\dot{\theta} + \dot{\nu})^2, \qquad (1)$$

where $m = m_1 + m_2 + m_t$ is a total mass, the dot represents the derivative with respect to time, $\mu_e = \frac{(m_1 + m_t/2)(m_2 + m_t/2)}{(m_1 + m_2 + m_t) - m_t/6}$ is a reduced mass, and ν is the true anomaly.

By summing the potential energies of the system's elements, noting that the tether length is very small compared to the radius of the mass's center, the system's potential energy, W, can be written on the form

$$W = -\frac{\mu m}{r_C} - \frac{\mu \mu_e l^2}{2 r_C^3}\left(3\cos^2\theta - 1\right), \qquad (2)$$

where μ is Earth's gravitational strength constant.

Using Eqs. (1) and (2), Lagrangian, L, can be constructed as $L = T - W$. The system's Lagrangian equations of motion have the form

$$\frac{d}{dt}\frac{\partial L}{\partial \dot{q}_i} - \frac{\partial L}{\partial q_i} = Q_i, \qquad (3)$$

where $q_i = \theta, l$ are generalized coordinates, and Q_i are not potential generalized forces.

Using the following nondimensional transformation $\frac{d(\,)}{dt} = \frac{d(\,)}{d\nu}\dot{\nu}, L = \frac{l}{l_r}$, equations of motion in nondimensional form can be written as

$$\theta'' + 2(\theta' + 1)\frac{L'}{L} + 3\cos\theta\sin\theta = \frac{Q_\theta}{\mu_e l^2 \dot{\nu}^2}, \qquad (4)$$

$$L'' - L\left[(\theta' + 1)^2 - 3\cos^2\theta + 1\right] = \frac{Q_l}{\mu_e \dot{\nu}^2}, \qquad (5)$$

the accent means a derivative with respect to the variable ν and $\dot{\nu}^2 = \mu / r_c^{\,3}$.

The system is under the influence of the Lorenz force resulting from the current flow through the tether interacting with the magnetic field and J_2 perturbation since the oblateness of Earth is considered. A non-tilted dipole model of the magnetic field is considered; its components in orbital frame, B_r, B_θ, and B_n, are determined as follows Stevens RE, (2008) :

$$B_r = -2\frac{\mu_m}{r_c^3}\sin\nu\sin i, \qquad (6)$$

$$B_\theta = \frac{\mu_m}{r_c^3}\cos\nu\sin i, \qquad (7)$$

$$B_n = \frac{\mu_m}{r_c^3}\cos i, \qquad (8)$$

where i is an orbital inclination and $\mu_m = 7.85\,10^{15}\ N/Am^2$, is the magnitude diploe

of Earth. It's assumed that a constant current, I, flows through the tether, and the magnetic field vector remains unchanged along the entire length. This constancy is attributed to the relatively small length of the tether compared to the system's mass radius. Following the principle of virtual work, the generalized electromagnetic torques $Q_{\theta e}, Q_{le}$, can be written in the form:

$$Q_{\theta,e} = -\frac{Il^2(m_2 - m_1)}{2(m_1 + m_2 + m_t)} B_n, \qquad (9)$$

$$Q_{l,e} = 0.$$

The effect of Earth's oblateness on the tethered satellite system can be evaluated using Earth's nonhomogeneous potential function, U, as mentioned in Kéchichian JA, (2021) as

$$U = \frac{\mu}{r_c}\left[1 - \sum_{n=2}^{\infty} J_n \left(\frac{R}{r_c}\right)^n P_n(\sin(\delta))\right], \qquad (10)$$

where J_n is a zonal harmonic of order n, R is Earth's equatorial radius, δ is the declination of the system's mass center to the equatorial plane, and $P_n(\sin(\delta))$ is the Legendre polynomial of order n in $\sin(\delta)$. Neglecting the J_3 and higher zonals, replacing $\sin(\delta)$ by z / r_c, and using the transformation matrix to the rotating frame, one can obtain the radial perturbation acceleration as

$$\boldsymbol{a}_{ob} = -\frac{3}{2}\frac{J_2 \mu R^2 \mathbf{r}_c}{r_c^5}\left(1 - 3\sin^2 i \sin^2 \nu\right). \qquad (11)$$

Follows Zhong R and Zhu Z, (2013) , the oblateness torque on the satellites caused by the acceleration is in the form

$$Q_{\theta,ob} = \gamma \sin(\theta) + \beta \sin(\theta)\cos(2\nu), \qquad (12)$$

where

$$\gamma = \chi.\left(1 - \frac{3\sin^2 i}{2}\right), \beta = \chi.\left(\frac{3\sin^2 i}{2}\right),$$

$$\chi = \left(\frac{3J_2 \mu R^2 l^2\left[m_2 M_m^2 - m_1(1 - M_m)^2\right]}{2r_c^5}\right), \qquad (13)$$

where $M_m = (m_1 + m_t / 2) / m.$

In this paper, we delve into the nonlinear dynamics of the pitch motion during the station-keeping phase, where the tether length remains constant. Substituting Eqs. (9), (12) into Eq. (4) with $L' = 0$, noting that $Q_\theta = Q_{\theta,e} + Q_{\theta,ob}$, gives

$$\theta'' + 3\cos\theta \sin\theta = \sigma_1 \sin\theta + \sigma_2 \sin\theta \cos 2\nu + \sigma_3, \qquad (14)$$

where

$$\sigma_1 = \sigma^*.\left(1 - \frac{3\sin^2 i}{2}\right), \sigma_2 = \sigma^*.\left(\frac{3\sin^2 i}{2}\right),$$

$$\sigma^* = \left(\frac{3J_2 R^2\left[m_2 M_m^2 - m_1(1 - M_m)^2\right]}{2\mu_e r_c^2}\right), \qquad (15)$$

$$\sigma_3 = -\frac{I(m_2 - m_1)\mu_m \cos i}{2m\mu_e \mu}.$$

One can see from Eq. (14) the electrodynamic tethered satellite system under Earth's oblateness is a nonlinear nonautonomous system.

Analysis of Chaotic Motion

In this section, the Melnikov function is employed to derive the necessary condition under which the dynamical system may exhibit a chaotic behavior.

Using $\boldsymbol{\theta} = (\theta_1, \theta_2)^T = (\theta, \dot{\theta})^T$, one can obtain the state equation of Eq. (14) as

$$\boldsymbol{\theta} = \boldsymbol{f}(\boldsymbol{\theta}) + \boldsymbol{g}(\boldsymbol{\theta}, \nu), \qquad (16)$$

with

$$\mathbf{f}(\boldsymbol{\theta}) = \begin{bmatrix} f_1 \\ f_2 \end{bmatrix} = \begin{bmatrix} \theta_2 \\ -3\sin\theta_1 \cos\theta_1 \end{bmatrix},$$

$$\mathbf{g}(\boldsymbol{\theta}, \nu) = \begin{bmatrix} g_1 \\ g_2 \end{bmatrix} = \begin{bmatrix} 0 \\ \sigma_1 \sin\theta_1 + \sigma_2 \sin\theta_1 \cos 2\nu + \sigma_3 \end{bmatrix}. \qquad (17)$$

The perturbation vector, $\mathbf{g}(\boldsymbol{\theta}, \nu) = \mathbf{g}(\boldsymbol{\theta}, \nu + p)$, is periodic of period $p = \pi$.

When $\mathbf{g}(\boldsymbol{\theta}, \nu) = 0$, the system corresponds to the unperturbed Hamiltonian case, with the first integral given by

$$\frac{1}{2}\theta_2^2 + \frac{3}{2}\sin^2\theta_1 = E, \qquad (18)$$

where a constant, E, represents the total kinetic energy of the system.

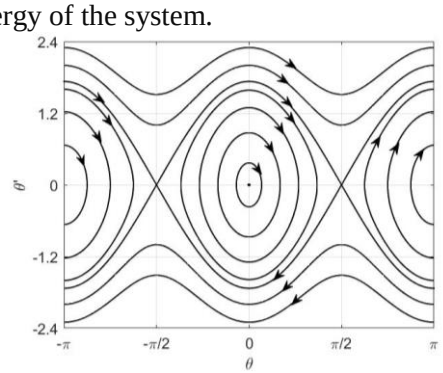

Fig. 2 Phase portrait of unperturbed system

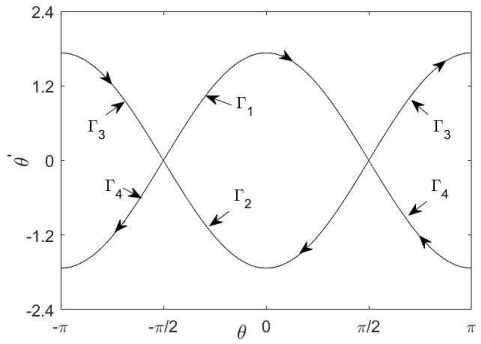

Fig. 3 Heteroclinic orbits

Figures (Fig. 2 and Fig. 3) present the phase portrait of the unperturbed system and the heteroclinic orbits that reach two different saddle points, $p_i = (\mp\pi/2, 0), i = 1, 2.$ The heteroclinic orbits can be written in the form Yu B et al., (2020)

$$\left(\theta_{10}^{\pm}(\nu), \theta_{20}^{\pm}(\nu)\right) = \left(\pm\sin^{-1}(\tanh(\sqrt{3}\nu)), \pm\sqrt{3}\,\mathrm{sech}(\sqrt{3}\nu)\right). \quad (19)$$

In the case of the perturbed system when $\mathbf{g}(\boldsymbol{\theta}, \nu) \neq 0$, near the equilibrium points, the heteroclinic orbits may split into unstable and stable manifolds. Chaos likely happens if these manifolds intersect transversally; according to Melnikov's analysis, the Melnikov function must have a simple zero (Yu B et al., (2022) ; Aslanov V, (2017)).

The Melnikov function is given by Aslanov VS, (2024)

$$M_{\pm}(\nu_0) = \int_{-\infty}^{+\infty} \boldsymbol{f}\left(\theta_0^{\pm}\right) \wedge \boldsymbol{g}\left(\theta_0^{\pm}, \nu + \nu_0\right) d\nu, \quad (20)$$

with $\nu_0 \in [0, p]$.

Substituting Eq. (17) into Eq. (20), using Eq. (19), yields

$$\begin{aligned} M_{\pm}(\nu_0) = \int_{-\infty}^{+\infty} & \left[\sigma_1 \sin\theta_{10}^{\pm}(\nu) + \sigma_2 \sin\theta_{10}^{\pm}(\nu)\right. \\ & \left.\cdot\cos 2(\nu + \nu_0) + \sigma_3\right] \theta_{20}^{\pm}(\nu)\, d\nu \\ = & \pm\sqrt{3}\sigma_1 \int_{-\infty}^{+\infty} \mathrm{sech}\left(\sqrt{3}\nu\right) \tanh\left(\sqrt{3}\nu\right) d\nu \\ & \pm\sqrt{3}\sigma_2 \int_{-\infty}^{+\infty} \mathrm{sech}\left(\sqrt{3}\nu\right) \tanh\left(\sqrt{3}\nu\right) \\ & \cos(2\nu)\, d\nu \cdot \cos 2\nu_0 \\ & \mp\sqrt{3}\sigma_2 \int_{-\infty}^{+\infty} \mathrm{sech}\left(\sqrt{3}\nu\right) \tanh\left(\sqrt{3}\nu\right) \\ & \sin(2\nu)\, d\nu \cdot \sin 2\nu_0 \\ & \pm\sqrt{3}\sigma_3 \int_{-\infty}^{+\infty} \mathrm{sech}\left(\sqrt{3}\nu\right) d\nu, \end{aligned} \quad (21)$$

calculating the integrals in Eq. (21), noting that when an odd function is integrated over a symmetrical interval gives zero. Under the mathematical condition, $\sin 2\nu_0$ ranges in the interval $[-1,1]$, the Melnikov function $M_{\pm}(\nu_0)$ has simple zeros if

$$\left|\frac{\sigma_3}{\sigma_2}\right| < 0.2881. \quad (22)$$

Eq. (22) gives the necessary, but not sufficient, condition under which the system may exhibit a chaotic motion near the saddle points.

According to Eqs. (15) and (22), the following four cases can be concluded

a) Case one: This is the case when both σ_2 and σ_3 vanish, the dynamical system equation represents the unperturbed case, which is plotted in Fig. 2 and Fig. 3.
b) Case two: This is the case when the system is perturbed only by the effect of the Lorenz force, i.e. $\sigma_3 \neq 0$ and $\sigma_2 = 0$, chaos doesn't occur since the condition, Eq. (22), is not satisfied.
c) Case three: This is the case when the J_2 effect constitutes the sole perturbation of the system, i.e. $\sigma_3 = 0$ and $\sigma_2 \neq 0$, chaos might occur since Eq. (22) is satisfied.
d) Case four: This is the case when the system is perturbed by both the Lorenz force and the oblateness acceleration, i.e. $\sigma_3 \neq 0$ and $\sigma_2 \neq 0$, chaos may be estimated using Eq. (22).

Numerical Results

This section presents a numerical simulation to verify the necessary condition, Eq. (22). The system's parameters are given as follows. The mother satellite mass, $m_1 = 1020\,Kg$, the subsatellite mass, $m_2 = 70\,Kg$, and the tether mass, $m_t = 3.4\,Kg$. The system orbits Earth in a circular orbit at an altitude of $600\,Km$, with an inclination of 63°.

One can note that σ_2 and σ_3 are dependent on the current passing through the tether, I, the inclination of the orbit, i, and the orbital altitude, H.

Firstly, at a specific altitude, using Eq. (22), the

chaotic zone in the parameter domain (I,i) is plotted in Fig. 4. The initial states of the system are $(\theta,\theta')=(-\pi/2+\pi/100,0)$, where $\pi/100$ is a given perturbed angle, positioning the system near one of the unstable saddle points $(\mp\pi/2,0)$. The point $(0.001,\pi/6)$ lies in the chaotic zone, which corresponds to the system's orbit having an inclination of $\pi/6$ with one mA current flowing through the tether. Fig. 5 presents a Poincaré section, indicating that the system is chaotic. Fig. 6 shows that the pitch motion angle is in irregular oscillation. If the orbit inclination is altered to $\pi/60$, the system is in a nonchaotic zone, which is described by Fig. 7 and Fig. 8, showing that the system is in a periodic motion.

Secondly, the chaotic zone in the parameter domain, (i,H), is plotted in Fig. 9 at $I=1mA$. The point $(\pi/6,900)$ lies in the nonchaotic zone. Fig. 10 being a Poincaré section, demonstrates that the system exhibits a periodic solution. Fig. 11 confirms this observation, showing that the pitch angle maintains a regular periodic oscillation with respect to the variable ν. When the inclination is adjusted to $\pi/60$, the system transitions into the chaotic zone. This transition is illustrated in Fig. 12, A Poincaré section corresponding to this state indicates that the system undergoes chaotic motion. Furthermore, Fig. 13 reveals that the pitch angle behaves as an irregular oscillator.

Finally, at an inclination of $\pi/30$, the chaotic region within the (I,H) parameter space is illustrated in Fig. 14. The point $(0.3\times10^{-4},600)$, lies within this chaotic region. Fig. 15 and Fig. 16 confirm this result, demonstrating that the system exhibits chaotic behavior. However, when the current flowing through the tether is increased to 0.3×10^{-2} the system no longer displays chaotic motion. Fig. 17 and Fig. 18 illustrate the resulting tumbling periodic motion of the system.

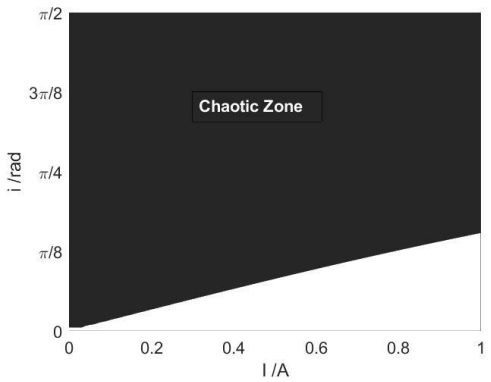

Fig. 4 Parameter domain for chaos

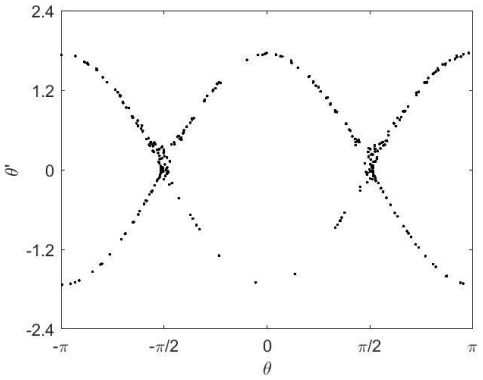

Fig. 5 Poincaré section

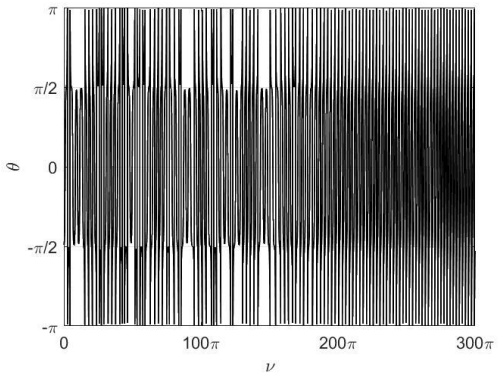

Fig. 6 Pitch angle versus ν

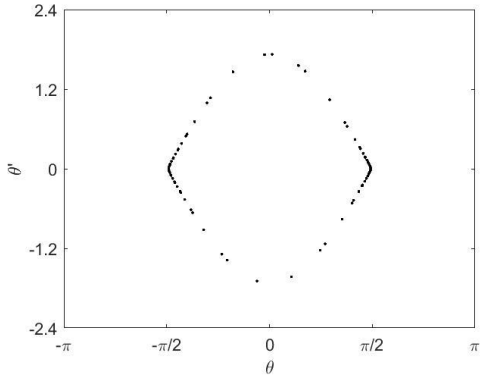

Fig. 7 Poincaré section

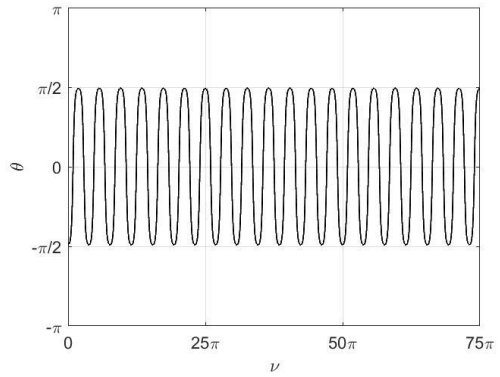

Fig. 8 Pitch angle versus υ

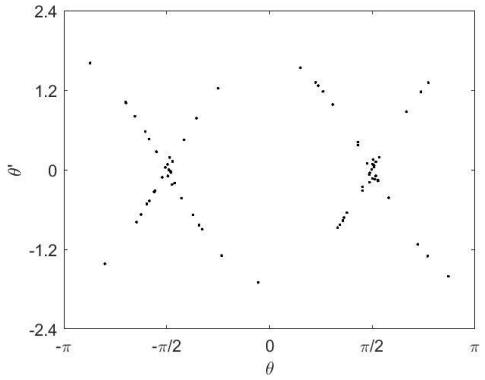

Fig. 12 Poincaré section

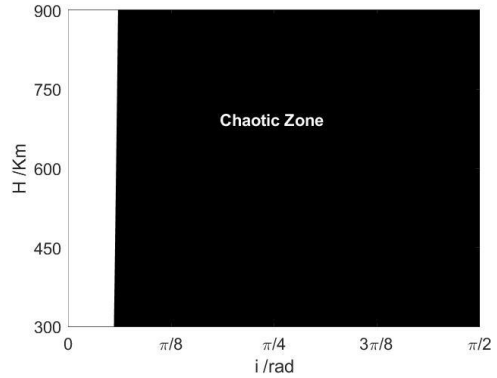

Fig. 9 Parameter domain for chaos

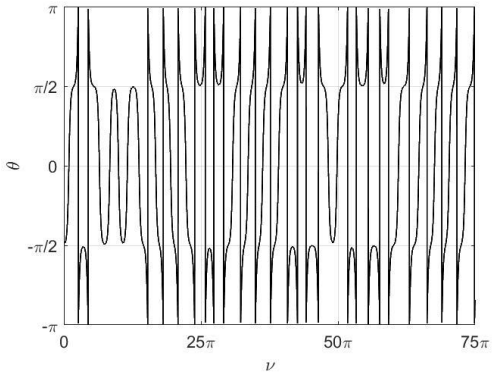

Fig. 13 Pitch angle versus ν

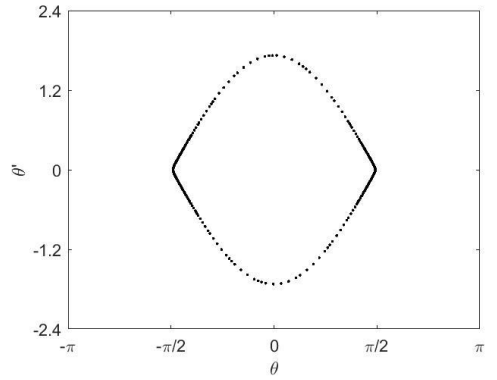

Fig. 10 Poincaré section

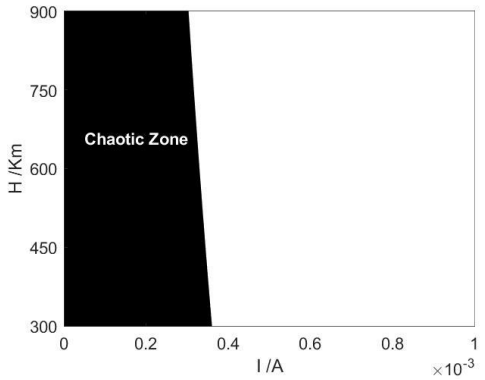

Fig. 14 Parameter domain for chaos

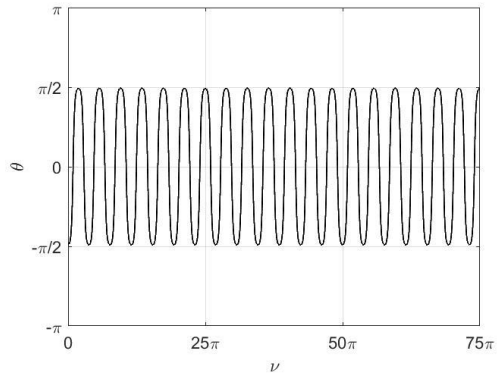

Fig. 11 Pitch angle versus υ

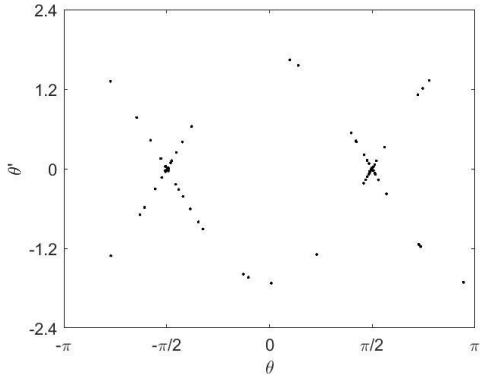

Fig. 15 Poincaré section

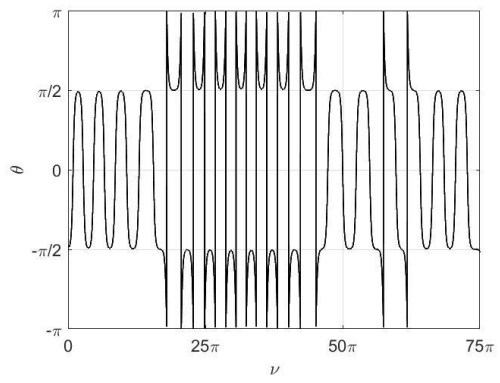

Fig. 16 Pitch angle versus υ

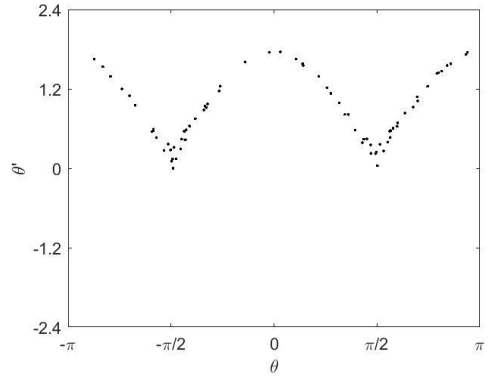

Fig. 17 Tumbling Poincaré section

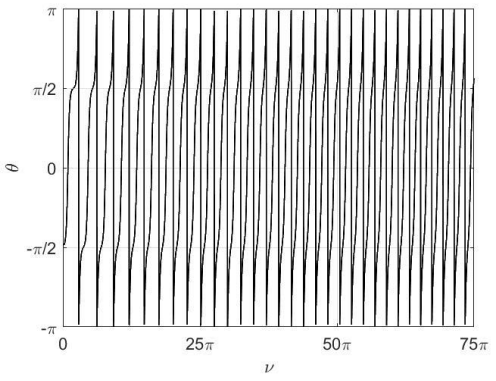

Fig. 18 Pitch angle versus υ

Conclusions

In this work, the chaotic motion of an electrodynamic tethered satellite system in a circular orbit under the influence of Earth's oblateness (J_2 effect) was analyzed. The system was modelled using a dumbbell configuration, representing two point masses connected by an inelastic tether. The equations of motion were derived via the Lagrangian approach, incorporating the effects of both the Lorentz force generated by the electrodynamic interaction and the radial acceleration due to Earth's oblateness.

To assess the potential for chaotic behavior, the Melnikov method was applied to establish a necessary condition for the onset of chaos. This condition enabled the identification of parameter domains in which chaotic motion is likely to occur. Numerical simulations were then conducted to validate the analytical predictions.

From the Melnikov-based analysis, three key scenarios emerged:

1. When the system is perturbed solely by the Lorentz force, chaotic motion does not occur.
2. When the perturbation arises solely from the oblateness effect, chaotic motion may arise.
3. When both the Lorentz force and oblateness effect are present, chaos may occur depending on whether the system parameters satisfy the necessary condition.

These findings indicate that the presence of the Lorentz force alone is insufficient to induce chaos, even in combination with the J_2 perturbation, unless the parameter values fall within the critical domain defined by the Melnikov analysis. This highlights the importance of carefully selecting system parameters to avoid unintended chaotic behavior in tethered satellite missions.

References

Ma X, and Wen H (2023) Deep learning for deorbiting control of an electrodynamic tether system. Acta Astronautica. 202: 26-33. https://doi.org/10.1016/j.actaastro.2022.10.019.

Razzaghi P, Al Khatib E, Bakhtiari S, and Hurmuzlu Y (2021) Real time control of tethered satellite systems to de-orbit space debris. Aerospace Science Technology. 109: 106379. https://doi.org/10.1016/j.ast.2020.106379.

Svotina V, and Cherkasova M (2023) Space debris removal–review of technologies and techniques. Flexible or virtual connection between space debris and service spacecraft. Acta Astronautica. 204: 840-853. https://doi.org/10.1016/j.actaastro.2022.09.027.

Liu J, Liu B, Wu Z, Jiang J, and Tian L (2020) Dynamics and potential applications of a lunar space tethered system. Acta Astronautica. 169: 138-149. https://doi.org/10.1016/j.actaastro.2020.01.021.

Liu J, and Mcinnes CR (2019) Resonant space tethered system for lunar orbital energy harvesting. Acta Astronautica. 156: 23-32. https://doi.org/10.1016/j.actaastro.2018.08.037.

Hu W, Song M, and Deng Z (2018) Energy dissipation/transfer and stable attitude of spatial on-orbit tethered system. Journal of Sound Vibration. 412: 58-73. https://doi.org/10.1016/j.jsv.2017.09.032.

Mashayekhi MJ, and Misra AK (2016) Effect of the finite size of an asteroid on its deflection using a tether–ballast system. Celestial Mechanics and Dynamical Astronomy. 125: 363-380. https://doi.org/10.1007/s10569-016-9687-y.

Zhong R, and Wang Y (2018) Dynamics and control of a probe tethered to an asteroid. Journal of Guidance, Control, and Dynamics. 41: 1585-1590. https://doi.org/10.2514/1.G003386.

Huang P, Zhang F, Chen L, Meng Z, Zhang Y, Liu Z, and Hu Y (2018) A review of space tether in new applications. Nonlinear Dynamics. 94: 1-19. https://doi.org/10.1007/s11071-018-4389-5.

Sanmartin JR, Lorenzini EC, and Martinez-Sanchez M (2010) Electrodynamic tether applications and constraints. Journal of Spacecraft and Rockets. 47: 442-456. https://doi.org/10.2514/1.45352.

Kumar K (2006) Review on dynamics and control of nonelectrodynamic tethered satellite systems. Journal of Spacecraft and Rockets. 43: 705-720. https://doi.org/10.2514/1.5479.

Modi V, Lakshmanan P, and Misra A (1990) Dynamics and control of tethered spacecraft-a brief overview. Paper presented at the Dynamics Specialists Conference. https://doi.org/10.2514/6.1990-1195.

Sánchez-Arriaga G, Lorenzini EC, and Bilén SG (2024) A review of electrodynamic tether missions: Historical trend, dimensionless parameters, and opportunities opening space markets. Acta Astronautica. https://doi.org/10.1016/j.actaastro.2024.09.002.

Hong AaT, Varatharajoo R, and Chak Y-C (2024) Review of deployment controllers for space tethered system. Advances in Space Research. https://doi.org/10.1016/j.asr.2024.11.061.

Andrievsky B, Popov AM, Kostin I, and Fadeeva J (2022) Modeling and control of satellite formations: A survey. Automation. 3: 511-544. https://doi.org/10.3390/automation3030026.

Aslanov V, and Ledkov A. (2012). Dynamics of tethered satellite systems: Elsevier.

Troger H, Alpatov A, Beletsky V, Dranovskii V, Khoroshilov V, Pirozhenko A, and Zakrzhevskii A. (2010). Dynamics of tethered space systems: CRC Press.

Zheng P, Cao X, and Zhang S (2008) J_2 perturbation effect on the deployment of tether-assisted deorbit system. Paper presented at the 2008 2nd International Symposium on Systems and Control in Aerospace and Astronautics. https://doi.org/10.1109/ISSCAA.2008.4776269.

Yu B, and Jin D (2010) Deployment and retrieval of tethered satellite system under J_2 perturbation and heating effect. Acta Astronautica. 67: 845-853. https://doi.org/10.1016/j.actaastro.2010.05.013.

Yu B, Jin D, and Wen H (2016) Nonlinear dynamics of flexible tethered satellite system subject to space environment. Applied Mathematics and Mechanics. 37: 485-500. https://doi.org/10.1007/s10483-016-2049-9.

Yu B, Xu S, and Jin D (2020) Chaos in a tethered satellite system induced by atmospheric drag and earth's oblateness. Nonlinear Dynamics. 101: 1233-1244. https://doi.org/10.1007/s11071-020-05844-8.

Yuan W, Deng H, and Liu J (2024) Chaotic libration and control of a space tether-sail system in earth polar orbits with J_2 perturbation. Applied Mathematical Modelling. 136: 115617. https://doi.org/10.1016/j.apm.2024.07.024.

Tikhonov A, Antipov K, Korytnikov D, and Nikitin DY (2017) Electrodynamical compensation of disturbing torque and attitude stabilization of a satellite in J_2 perturbed orbit. Acta Astronautica. 141: 219-227. https://doi.org/10.1016/j.actaastro.2017.10.009.

Stevens RE. (2008). Optimal control of electrodynamic tether satellites. (Ph.D. Ph.D.), Air Force Institute of Technology,

Kéchichian JA. (2021). Orbital relative motion and terminal rendezvous: Springer.

Zhong R, and Zhu Z (2013) Libration dynamics and stability of electrodynamic tethers in satellite deorbit. Celestial Mechanics and Dynamical Astronomy. 116: 279-298. https://doi.org/10.1007/s10569-013-9489-4.

Yu B, Tang Y, and Ji K (2022) Chaotic behaviors of an in-plane tethered satellite system with elasticity. Acta Astronautica. 193: 395-405. https://doi.org/10.1016/j.actaastro.2022.01.024.

Aslanov V. (2017). Rigid body dynamics for space applications: Butterworth-Heinemann.

Aslanov VS (2024) Suppressing chaotic oscillations of a tether anchored to the phobos surface under the l1 libration point. Chaos, Solitons and Fractals. 181: 114663. https://doi.org/10.1016/j.chaos.2024.114663.

Scientific Journal for Damietta Faculty of Science **15**(2) 2025, 191-191
Doi: 10.21608/sjdfs.2025.399892.1240
ISSN Print 2314-8594
ISSN Online 2314-8616

https://sjdfs.journals.ekb.eg/

الملخص العربي

عنوان البحث: الحركة الفوضوية لنظام قمر صناعي كهروديناميكي مربوط تحت تأثير تفلطح الأرض في مدار دائري

أحمد يوسف*[١]، أحمد مجدي عبد العزيز[٢]، عبد الحكيم أبو الفتوح عبد النبي[١]، يحيى أحمد عبد العزيز

[١]قسم الرياضيات، كلية العلوم، جامعة دمياط، دمياط، مصر.
[٢] المركز القومي لبحوث الفلك والجيوفيزياء (NRIAG)، القاهرة، مصر.

يتناول هذا البحث دراسة السلوك الفوضوي لنظام قمر صناعي كهروديناميكي مربوط يتحرك في مستوى المدار تحت تأثير تفلطح الأرض (معامل J_2) تم نمذجة النظام باستخدام نموذج الدمبل، والذي يمثل كتلتين نقطيتين متصلتين بواسطة حبل غير مرن. تم اشتقاق معادلات الحركة باستخدام منهج لاغرانج، بعد احتساب العزوم الناتجة عن قوة لورنتز والتسارع الشعاعي الناتج عن التفلطح الأرضي.

تم تطبيق تحليل ميلنيكوف لاشتقاق شرط ضروري لحدوث الحركة الفوضوية، مما أتاح تحديد مجالات القيم التي قد يظهر فيها هذا السلوك. كما تم دعم النتائج التحليلية بمحاكاة عددية تؤكد صحة هذا الشرط.

أظهرت النتائج ثلاث حالات رئيسية:

١. عند وجود قوة لورنتز فقط، لا يحدث سلوك فوضوي.
٢. عند وجود تأثير التفلطح فقط، قد يحدث سلوك فوضوي.
٣. عند وجود كلا التأثيرين معًا، فإن حدوث الفوضى يعتمد على تحقيق الشرط الضروري الذي تم التوصل إليه باستخدام تحليل ميلنيكوف.

تشير هذه النتائج إلى أن وجود قوة لورنتز وحدها لا يكفي لإحداث الفوضى، حتى مع وجود تأثير J_2 ، ما لم تكن المعلمات ضمن المجال الحرج الذي تم تحديده. وتبرز هذه الدراسة أهمية اختيار معلمات النظام بعناية لتجنب السلوك الفوضوي غير المرغوب فيه في تطبيقات الأقمار الصناعية المربوطة.